applied sciences

MDPI

Article

Mechanistic Study of the Influence of Reactant Type and Addition Sequence on the Microscopic Morphology of α-Al_2O_3

Weixiang Wen, Yang Bai *, Mengxu Xu, Yujuan Gao, Pingke Yan * and Huabing Xu

School of Resources and Environmental Engineering, Shandong University of Technology, Zibo 255000, China; wwx17852036423@163.com (W.W.); xumengxu666@163.com (M.X.); gaoyujuan0122@163.com (Y.G.); huabing_sdut@163.com (H.X.)

* Correspondence: by9211@163.com (Y.B.); yanpingke@126.com (P.Y.)

Abstract: To perform an in-depth study of the crystal growth habits and phase changes of alumina and its precursors in reaction systems, this paper studied the effects of reactant type and addition order on the morphology of alumina using hydrothermal methods with different precipitants and aluminum sources as reactants. Research has shown that sodium bicarbonate and ammonium bicarbonate can be used as precipitants to prepare adhered spherical alumina and irregular short rod alumina, while potassium bicarbonate can be used as a precipitant to prepare hexagonal flake alumina. Using aluminum sulfate octahydrate, aluminum chloride hexahydrate, and aluminum nitrate, nine hydrates were prepared as aluminum sources, and agglomerated alumina, irregular short rod-shaped alumina, and fused alumina were obtained. The order of reactant addition affects the precursor phase of alumina, thereby affecting the microstructure of alumina after calcination, resulting in flake alumina with pores and short rod alumina. The results of this paper will provide theoretical guidance for the preparation of alumina with different micromorphologies.

Keywords: α-Al_2O_3; microscopic morphology; reactant types; addition sequence; ammonium aluminum carbonate hydroxide; Boehmite

check for updates

Citation: Wen, W.; Bai, Y.; Xu, M.; Gao, Y.; Yan, P.; Xu, H. Mechanistic Study of the Influence of Reactant Type and Addition Sequence on the Microscopic Morphology of α-Al_2O_3. *Appl. Sci.* **2024**, *14*, 2438. https://doi.org/10.3390/app14062438

Academic Editor: Roberto Bergamaschini

Received: 17 January 2024
Revised: 1 March 2024
Accepted: 12 March 2024
Published: 14 March 2024

Copyright: © 2024 by the authors. Licensee MDPI, Basel, Switzerland. This article is an open access article distributed under the terms and conditions of the Creative Commons Attribution (CC BY) license (https://creativecommons.org/licenses/by/4.0/).

1. Introduction

α-Alumina, commonly known as corundum, belongs to the trigonal crystal system. In its structure, oxygen atoms can be approximately considered hexagonally close-packed, while aluminum atoms are uniformly distributed in octahedral coordination centers surrounded by oxygen atoms. Compared to β-alumina and γ-alumina, α-alumina has the tightest crystal structure, highest chemical stability, and excellent electrochemical properties and corrosion resistance. It is widely used in areas such as integrated circuits [1,2], optical sensing [3,4], filler materials [5], and refractory materials [6,7]. The importance of the microstructure on the application performance of materials is well known. Altering the microstructure of α-alumina (referred to as alumina) can broaden the application range of alumina. For instance, flake alumina exhibits a small thickness and a large diameter-to-thickness ratio, reaching the nanometer level in the thickness direction and the micron level in the radial direction. This dual functionality at both the nanometer and micron scales makes it widely applicable in diverse fields, such as in pigments, cosmetics, and abrasives [8,9]. Mesoporous alumina, which is characterized by a high specific surface area, suitable pore structure, narrow pore size distribution, and excellent surface acid resistance, has shown utility as an adsorbent, catalyst, or catalyst carrier in the energy and chemical industries [10].

The various alumina production methods can be categorized into three main groups. The solid-phase method demonstrates high efficiency in alumina production. However, there are limitations regarding the particle sizes, purities, and morphologies of the powders due to constraints imposed by the equipment and processes. This often results in powders that are not sufficiently fine and are prone to impurity contamination. Xu et al. [11]

synthesized highly stable active alumina using the low-temperature solid-phase precursor method. The alumina, even after treatment at 1100 °C for 4 h, maintained the γ-phase, with a specific surface area of 92 m^2/g and a pore volume of 0.68 cm^3/g. Shen et al. [12] prepared alumina powder using the solid-phase sintering method. Their study found that the addition of NH_4F additive reduced the phase transition temperature of α-alumina by about 300 °C, resulting in the crystallization of alumina crystals in a platelet growth manner. On the other hand, the addition of NH_4Cl additive had a relatively minor effect on the transformation temperature and impurity content of α-alumina, resulting in alumina particles with a mixture of worm-like and platelet-like morphologies. The gas-phase method has stringent requirements for airtight equipment during production. Owing to its high production cost and low yield, this method is still in the laboratory research stage and has not achieved mass production. Bogdan Stefan Vasile et al. [13] introduced the application of ceramic composite materials prepared by electron beam physical vapor deposition (EB-PVD) in the aerospace industry. They discussed the surface coating of aerospace materials with alumina–zirconia composite coatings, characterized by an exceptionally high melting point of approximately 2700 °C, excellent mechanical properties, and stability under oxidative conditions. Fabian Konstantiniuk et al. [14] synthesized polycrystalline α-Al_2O_3 coatings via thermal activated chemical vapor deposition (CVD). Due to the advantageous combination of the chemical inertness, thermal stability, and high thermal hardness of alumina coatings, they are widely used as wear-resistant hard coatings to protect cutting tools in the metal cutting industry. Compared to the other two methods, the liquid-phase method has significant advantages in controlling the micromorphology of alumina. Among these methods, hydrothermal methods can be used to control the particle sizes and microstructures of products by changing the hydrothermal reaction conditions, such as the reactant type, temperature, concentration, and pH of the reaction system, and by adding crystallization control agents to obtain particles with good dispersion and uniform sizes [15–17]. Additionally, hydrothermal methods are characterized by their low cost, simple operation, and ease of industrial production. As a result, the use of these materials has gradually become common for producing high-purity ultrafine alumina.

Currently, research on the morphology control of alumina produced by hydrothermal methods has focused mainly on factors such as the type of crystal modifier, the presence of seed crystals, and the pH of the reaction system. There is comparatively less research on the types of raw materials and their additional sequences. However, adjusting the addition sequence of reactants can lead to changes in the product morphology. For example, Chang et al. [18] studied the effect of different feeding orders on the morphology of sheet-like mordenite and reported that changing the order of reagent addition facilitated mordenite formation. Zhang et al. [19] optimized the preparation of T-type zeolite membranes by changing the dosing sequence to prepare zeolite membranes with larger, more uniform, and complete crystal sizes. Liu et al. [20] changed the order of raw material addition to prepare samples with regular spherical shapes, small and uniform grain sizes, and good dispersibility.

The types of reactants and the sequence of their addition strongly influence the microstructure of the resulting products. To synthesize aluminum oxide products with uniform particle sizes and controllable morphologies, this study plans to use eighteen-water aluminum sulfate, hexahydrate aluminum chloride, and nonahydrate aluminum nitrate as aluminum sources. Ammonium bicarbonate, sodium bicarbonate, and potassium bicarbonate were employed as precipitants. The hydrothermal method was utilized to synthesize precursors, and aluminum oxide powder was prepared through calcination. This study aimed to investigate the influence of the type of reactant and the order of addition on the microstructure of aluminum oxide. The research results will provide theoretical guidance for the controlled synthesis of aluminum oxide with different microstructures.

2. Materials and Methods

2.1. Raw Materials and Instruments

The experimental raw materials mainly included aluminum sulphate octadecahydrate, aluminum chloride hexahydrate, nonahydrate aluminum nitrate, ammonium bicarbonate, sodium bicarbonate, and potassium bicarbonate, all of which were of analytical purity and obtained from Sinopharm Group Co., Ltd. (Shanghai, China).

The experimental equipment used included a freeze dryer (Scienz-12n, Ningbo Scientz Biotechnology Co., Ltd., Ningbo, China), hydrothermal reactor (sh-100 mL, Suzhou Shenghua Instrument Technology Co., Ltd., Suzhou, China), muffle furnace (ksl-1400x, Hefei Kejing Materials Technology Co., Ltd., Hefei, China), high-speed desktop centrifuge (h1850, Hunan Xiangyi Laboratory Instrument Development Co., Ltd., Changsha, China), electric blast drying oven (fn101-3a, Beijing ever bright medical treatment instrument Co., Ltd., Beijing, China), X-ray diffractometer (RIGAKU Ultima IV, Rigaku Corporation, Showa, Japan), scanning electron microscope (Zeiss Gemini 300, Carl Zeiss AG, Oberkochen, Germany), Fully Automatic Surface Area and Porosity Analyzer (Micromeritics ASAP 2460, Micromeritics Instrument Ltd., Atlanta, GA, USA) and Thermal Analyzer (Netzsch STA2500, NETZSCH-Gerätebau GmbH, Selbu, Germany).

2.2. Experimental Methods

(1) Precipitates (ammonium bicarbonate, sodium bicarbonate, and potassium bicarbonate) were prepared at a concentration of 1.2 mol/L, and aluminum sources (aluminum sulfate, aluminum chloride, and aluminum nitrate) were prepared at a concentration of 0.4 mol/L. (2) Fifty milliliters of the aluminum source solution was added dropwise to 50 mL of the precipitant solution at a rate of 10 mL/min while stirring vigorously for 30 min. (3) The stirred reaction mixture was transferred to a hydrothermal reaction kettle lined with polytetrafluoroethylene (PTFE) and crystallized at 150 °C for 12 h. (4) After crystallization, the hydrothermal reaction products were washed three times by centrifugation with deionized water. A freeze dryer was subsequently used for drying. (5) The dried product was heated at a ramp rate of 5 °C/min to 1000 °C, and the temperature was maintained for 2 h for calcination. The final aluminum oxide product was obtained after natural cooling.

2.3. Sample Morphology and Crystal Structure Testing and Characterization

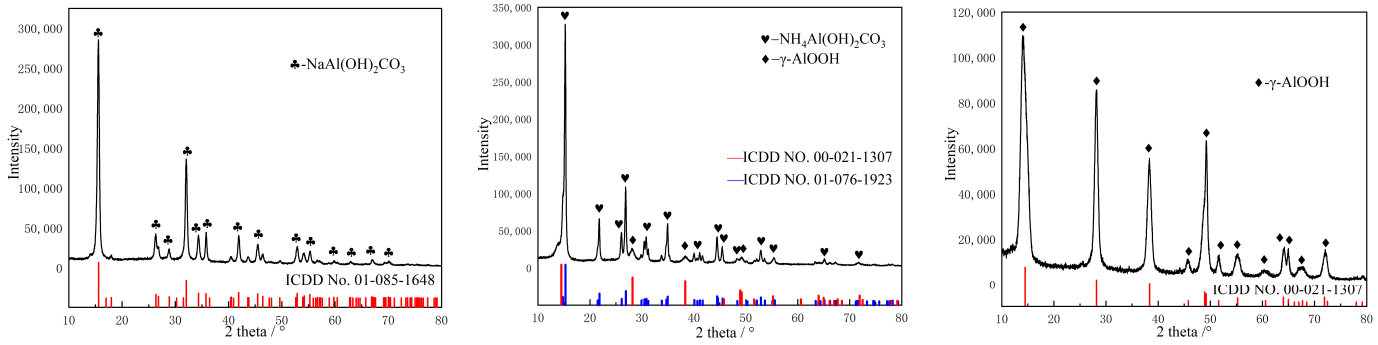
The phase composition and crystal structure of the products were qualitatively analyzed using an Ultima IV X-ray powder diffractometer. The testing parameters were as follows: Cu target Kα X-ray radiation, scanning voltage of 40 kV, scanning current of 30 mA, step size of 0.02°, and scanning angle ranging from 10° to 80°. The morphology and size of the products were observed using a Gemini 300 scanning electron microscope. The testing parameters were as follows: Schottky field emission electron gun, with a resolution of 1.0 nm @ 15 kV, 1.6 nm @ 1 kV. The accelerating voltage ranges from 0.02 to 30 kV, with a probe current of 3 pA to 20 nA, and magnification ranging from 10x to 1,000,000x. The BET surface areas, average pore size, and the nitrogen gas uptake isotherms were determined through N_2 adsorption–desorption experiments using Micromeritics ASAP 2460 instrument at 77 K. The results of the thermogravimetric experiments were obtained using the NETZSCH STA 2500 (STA2500A-0418-N) instrument, with a temperature range of 30 °C to 1000 °C, a heating rate of 20 °C per minute, and under a nitrogen atmosphere.

3. Results and Discussion

3.1. Effect of Precipitant Type on the Morphology of Alumina Precursors

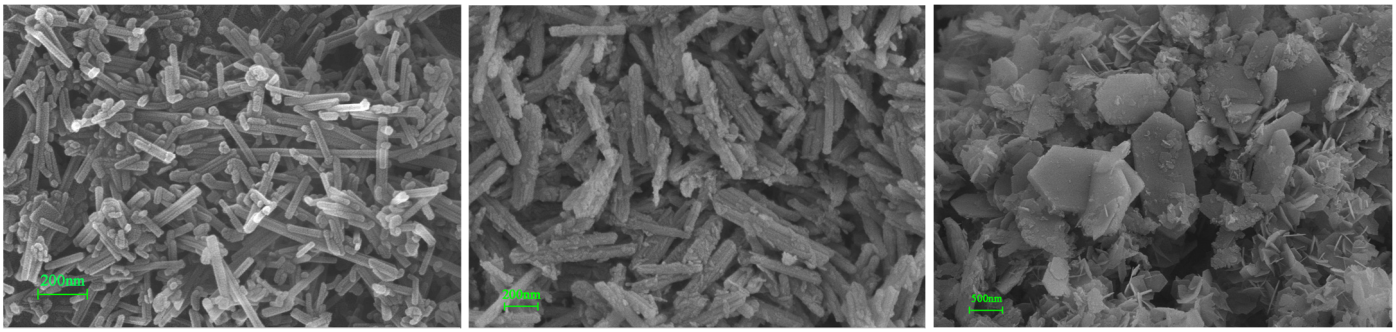
The morphology of alumina exhibits an inheritance relationship with its precursor morphology. To investigate the influence of the precipitant type on the morphology of the aluminum oxide, XRD and SEM analyses were conducted on the precursor products prepared with the three different precipitants. Using hexahydrate aluminum chloride as

the aluminum source, the experimental procedures were the same as those outlined in Section 2.2. The test results are presented in Figures 1 and 2, respectively.



(**a**) (**b**) (**c**)

Figure 1. XRD patterns of alumina precursors prepared from different precipitants. (**a**) Sodium bicarbonate; (**b**) ammonium bicarbonate; (**c**) potassium bicarbonate.



(**a**) (**b**) (**c**)

Figure 2. SEM images of alumina precursors prepared from different precipitants. (**a**) Sodium bicarbonate; (**b**) ammonium bicarbonate; (**c**) potassium bicarbonate.

The XRD spectra results indicate that aluminum oxide precursors prepared with sodium bicarbonate and potassium bicarbonate as precipitants do not exhibit any additional peaks. However, aluminum oxide precursor prepared with ammonium bicarbonate as the precipitant primarily consists of ammonium aluminate carbonate, with additional peaks attributed to γ-AlOOH. The detailed peak positions and crystal planes in the XRD spectrum are shown in Table 1.

Table 1. XRD refinement. $NaAl(OH)_2CO_3$(ICDD 00-045-1359), $NH_4Al(OH)_2CO_3$(ICDD 01-076-1923), and γ-AlOOH(ICDD 00-021-1307).

Mineral Name	Peaks and Theta (2θ)
$NaAl(OH)_2CO_3$	15.6°, 26.3°, 26.8°, 28.8°, 32.1°, 34.5°, 35.8°, 41.9°, 45.4°, 46.4°, 52.8°, 54.1°, 55.2°, 66.9°, 70.0° (011), (020), (112), (013), (121), (004), (211), (220), (015), (105), (231), (125), (224), (440), (051)
$NH_4Al(OH)_2CO_3$	14.8°, 15.2°, 21.8°, 26.0°, 26.9°, 30.4°, 30.8°, 34.7°, 34.9°, 40.0°, 41.1°, 44.4°, 44.6°, 45.5°, 52.9°, 55.4° (020), (110), (111), (130), (200), (131), (220), (221), (112), (150), (132), (222), (311), (060), (312), (400)
γ-AlOOH	14.4°, 28.1°, 38.3°, 45.7°, 48.9°, 49.2°, 51.5°, 55.2°, 60.5°, 64.0°, 64.9°, 67.6°, 71.9°, 72.4° (020), (120), (031), (131), (051), (200), (220), (151), (080), (231), (002), (171), (251), (122)

The average crystal size (D) of different precursors of aluminum oxide prepared in different addition sequences was determined using Scherrer's formula, $D = k\lambda/(B\cos\theta)$, where k is the constant value of 0.9; λ is the wavelength of X-ray radiation; B and θ

are, respectively, the full width at half maximum (FWHM) and half of the diffraction angle (2θ) detected on the crystal face in the XRD spectrum. The precursor prepared with sodium bicarbonate is sodium basic aluminate carbonate, with an average crystal grain size of 19.96 nm; the precursor prepared with ammonium bicarbonate is sodium basic aluminum ammonium carbonate, with an average crystal grain size of 20.03 nm; the precursor prepared with potassium bicarbonate is boehmite, with an average crystal grain size of 22.53 nm. The average grain size of alumina precursors prepared with different precipitants is shown in Table 2.

Table 2. Average crystal grain size of aluminum oxide precursors prepared with different precipitants. (a) Sodium bicarbonate; (b) ammonium bicarbonate; (c) potassium bicarbonate.

Precipitants	Lattice Parameters (Å)	Average Crystalline Size, D (nm)
(a)	$NaAl(OH)_2CO_3$ (a = 3.7, b = 12.2, c = 2.8)	19.96
(b)	γ-AlOOH (a = 3.7, b = 12.2, c = 2.8) $NH_4Al(OH)_2CO_3$(a = 6.6, b = 11.9, c = 5.7)	20.03
(c)	γ-AlOOH (a = 3.7, b = 12.2, c = 2.8)	22.53

Figures 1 and 2 show that, when sodium bicarbonate was used as the precipitant, the prepared precursor exhibited a rod-shaped sodium basic aluminum carbonate ($NaAl(OH)_2CO_3$) with an average length of 800 nm. During the reaction process, sodium bicarbonate first reacts with aluminum chloride to form boehmite (γ-AlOOH). Subsequently, sodium bicarbonate further reacts with boehmite, ultimately yielding sodium basic aluminum carbonate, as indicated by the chemical reaction in Equations (1) and (2).

$$AlCl_3 + 3NaHCO_3 = \gamma\text{-}AlOOH \downarrow + 3NaCl + 3CO_2 \uparrow + H_2O \quad (1)$$

$$\gamma\text{-}AlOOH + NaHCO_3 = NaAl(OH)_2CO_3 \quad (2)$$

When ammonium bicarbonate was used as the precipitant, the prepared precursor appeared as irregular rod-shaped sodium basic aluminum ammonium carbonate ($NH_4Al(OH)_2CO_3$). The crystal length was similar to that of sodium basic aluminum carbonate, but the diameter increased, and the surface exhibited a rough texture. This is because, compared to sodium basic aluminum carbonate, sodium basic aluminum ammonium carbonate showed characteristic peaks of the (111) crystal plane with higher intensity, indicating preferential growth of the (111) crystal plane in the sodium basic aluminum ammonium carbonate crystals. Therefore, the crystals of sodium basic aluminum ammonium carbonate had a larger diameter than did those of sodium basic aluminum carbonate [21]. During the reaction process, ammonium bicarbonate directly reacted with aluminum chloride to produce sodium basic aluminum ammonium carbonate. Due to the poor stability of sodium basic aluminum ammonium carbonate under high-temperature conditions, some of the sodium basic aluminum ammonium carbonate decomposed into boehmite during the crystallization process, resulting in a rough surface on the crystals. This was evidenced by the appearance of characteristic peaks of boehmite in the XRD spectrum, as indicated by the chemical reaction in Equations (3) and (4).

$$AlCl_3 + 4NH_4HCO_3 = NH_4Al(OH)_2CO_3 \downarrow + 3NH_4Cl + 3CO_2 \uparrow + H_2O \quad (3)$$

$$NH_4Al(OH)_2CO_3 = \gamma\text{-}AlOOH + NH_3 \cdot H_2O + CO_2 \uparrow \quad (4)$$

Sodium bicarbonate and potassium bicarbonate share similar properties. When potassium bicarbonate was used as the precipitant, in the reaction system, potassium bicarbonate first reacted with aluminum chloride to form boehmite. Due to the larger radius of potassium ions, boehmite cannot react with potassium bicarbonate. Therefore, the precursor only contained boehmite as the phase. The characteristic peak of boehmite in the XRD

spectrum had a wider half-peak width, indicating a finer crystal particle size. The reaction process is illustrated by the chemical reaction in Equation (5).

$$AlCl_3 + 3KHCO_3 = \gamma\text{-}AlOOH \downarrow + 3KCl + 3CO_2 \uparrow + H_2O \quad (5)$$

From Figure 3a, it can be observed that the TG curve sharply decreases starting at 309.8 °C, indicating the thermal decomposition of carbonate ions. A slight decrease in the TG curve is observed at 711 °C, which may be attributed to the removal of water molecules with different binding energies in the aluminum oxide precursor. The DTG curve in Figure 3b reveals that the mass change before 279 °C is due to the removal of adsorbed water and thermal decomposition. After 279 °C, the mass change is attributed to the removal of crystalline water from the aluminum oxide precursor. As depicted in Figure 3c, the DTG curve shows two peaks at 100 °C and 300 °C, which are likely caused by the removal of excess water molecules from the surface and interlayers of boehmite. The sharp decrease in the TG curve at 409 °C indicates the transformation of boehmite into γ-alumina. Based on the three TG curves, it can be inferred that aluminum aluminate carbonate is more readily converted to α-alumina compared to boehmite and sodium aluminate carbonate.

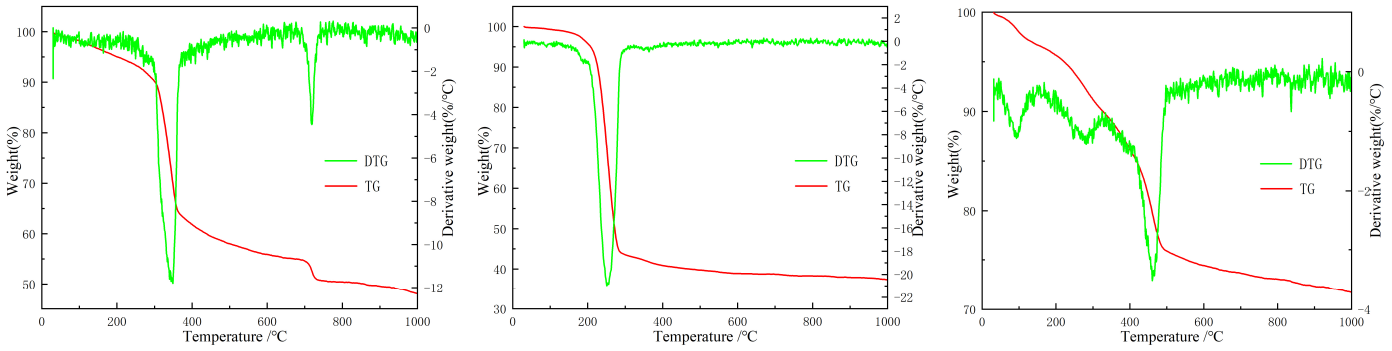


Figure 3. The TG-DTG curves of alumina precursors prepared from different precipitants. (**a**) Sodium bicarbonate; (**b**) ammonium bicarbonate; (**c**) potassium bicarbonate.

3.2. Influence of Precipitant Type on the Morphology of the Aluminum Oxide

To further investigate the influence of the precursors on the microstructure of the aluminum oxide, SEM analysis was conducted on the products obtained after calcination of the precursors prepared with different precipitants. The test results are shown in Figure 4.

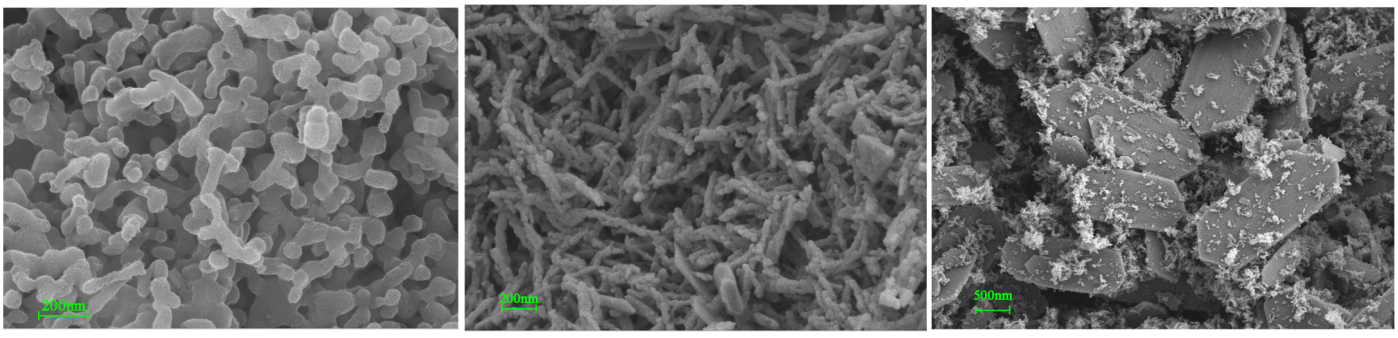


Figure 4. SEM images of alumina prepared with different precipitants. (**a**) Sodium bicarbonate; (**b**) ammonium bicarbonate; (**c**) potassium bicarbonate.

Figure 4 shows that, when sodium bicarbonate was used as the precipitant, the precursor sodium basic aluminum carbonate underwent high-temperature calcination, resulting in the formation of fused aluminum oxide with an average particle size of 80 nm. The aluminum oxide particles were interconnected and exhibited poor dispersion. This is attributed to the thermal decomposition of sodium basic aluminum carbonate during high-temperature calcination, which generates a significant amount of sodium oxide [22]. Sodium oxide acts as a fluxing agent, causing the rod-shaped precursor to melt and ultimately form a fused state with mutual adhesion, as indicated by the chemical reaction in Equation (6). The experimentally prepared fused alumina and rod-shaped alumina, due to their abundant porosity, excellent hardness, and wear resistance, along with their stable chemical properties, can disperse active substances on their surface and within their pores. They are suitable for applications in petroleum processing, catalytic cracking, and other fields. When ammonium bicarbonate was used as the precipitant, the precursor, sodium basic aluminum ammonium carbonate, contained a large amount of ammonium ions, carbonate ions, and hydroxyl groups. During the formation of aluminum oxide through high-temperature calcination, these ions not only had spatial filling effects but also contributed to the formation of aluminum oxide with a greater pore volume and larger pore size due to the gas-expanding pore-forming effect. The rod-shaped precursor structure was disrupted, and the microstructure of the aluminum oxide appeared as irregular short rods, as indicated by the chemical reaction in Equation (7). When potassium bicarbonate was used as the precipitant, the precursor boehmite underwent thermal decomposition. Due to the limited gas generation, the hexagonal precursor structure remained intact, and the microstructure of the aluminum oxide still predominantly consisted of hexagonal plates, as indicated by the chemical reaction in Equation (8). The experimentally prepared platelet alumina can serve as a filler, playing a crucial role in ceramics, plastics, and rubber products. It enhances hardness and adjusts the coefficient of thermal expansion, while its corundum structure improves heat resistance. Platelet alumina also possesses good dispersibility and parallel alignment, making it suitable for polishing powders. It enables the surface to be nearly parallel to the material being polished, minimizing surface damage, and maintaining a smooth, mirror-like finish after polishing.

$$2NaAl(OH)_2CO_3 = Al_2O_3 + 2CO_2 \uparrow + 2H_2O + Na_2O \quad (6)$$

$$2NH_4Al(OH)_2CO_3 = Al_2O_3 + 2CO_2 \uparrow + 3H_2O + 2NH_3 \uparrow \quad (7)$$

$$2\gamma - AlOOH = Al_2O_3 + H_2O \quad (8)$$

The N_2 adsorption–desorption results are shown in Figure 5. The curves in the N_2 adsorption–desorption isotherm plot exhibit a type IV adsorption branch with an H3 hysteresis loop. According to the BJH calculation, as shown in the pore size distribution curve, these shapes indicate the presence of a significant amount of mesopores. The specific surface area of alumina prepared with ammonium bicarbonate (68.54 m^2/g) is higher than that prepared with potassium bicarbonate (27.07 m^2/g) and sodium bicarbonate (6.34 m^2/g). This indicates that alumina prepared with ammonium bicarbonate possesses abundant active sites and superior adsorption capacity.

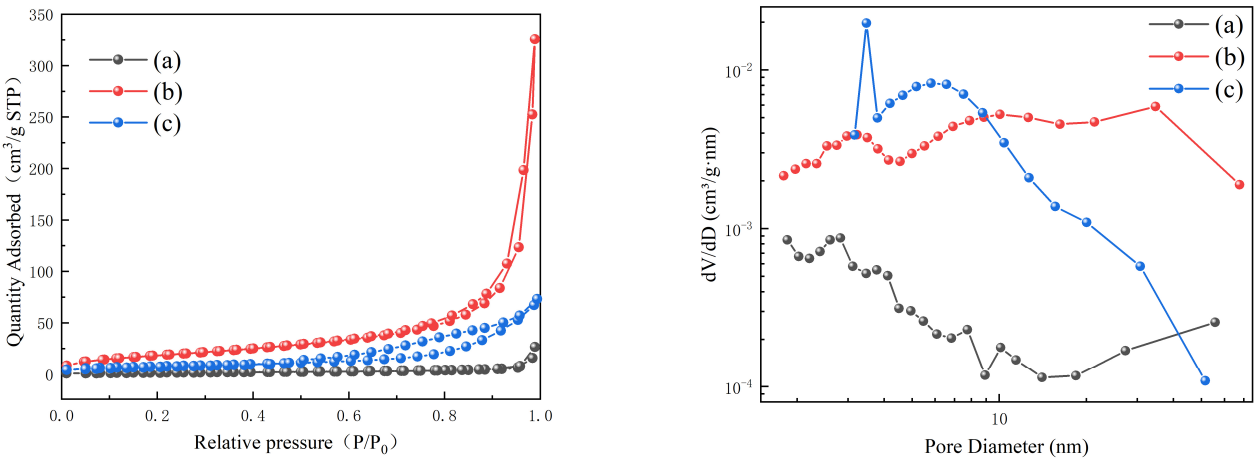
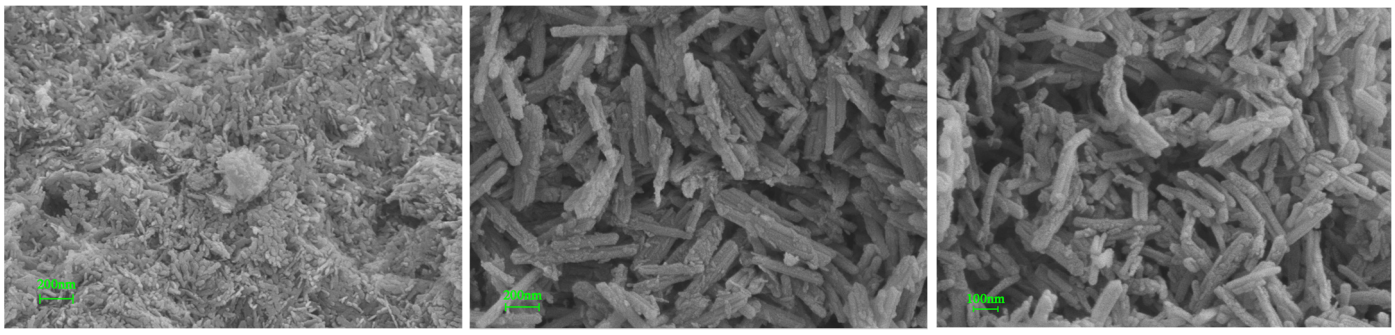


Figure 5. N_2 adsorption–desorption isotherms and BJH pore size distribution plots of alumina prepared with different precipitants. (a) Sodium bicarbonate; (b) ammonium bicarbonate; (c) potassium bicarbonate.

3.3. Impact of the Aluminum Source Type on the Precursor Morphology of the Aluminum Oxides

Using eighteen-water aluminum sulfate, hexahydrate aluminum chloride, and nonahydrate aluminum nitrate as aluminum sources and ammonium bicarbonate as the precipitant, the impact of aluminum source types on the morphology of aluminum oxide was investigated. Initially, XRD and SEM analyses were performed on the precursor products obtained from the three aluminum sources. The test results are presented in Figure 6 and Figure 7, respectively.



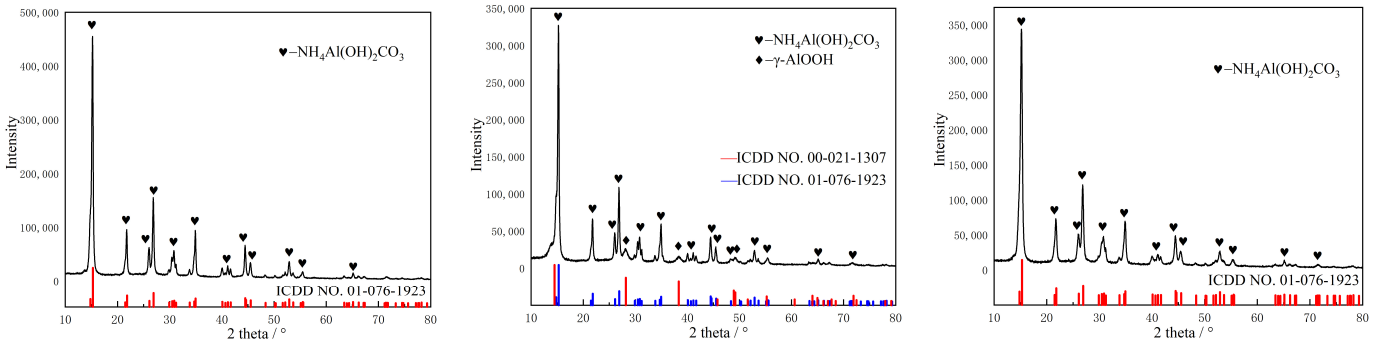
(**a**) (**b**) (**c**)

Figure 6. SEM images of alumina precursors prepared from different aluminum sources. (**a**) Aluminum sulfate; (**b**) aluminum chloride; (**c**) aluminum nitrate.

It is evident from Figure 6 that the precursors prepared from different aluminum sources exhibit a rod-like morphology. From Figure 7 and Table 1, it can be observed that aluminum oxide precursors prepared with aluminum sulfate and aluminum nitrate as the aluminum source result in pure-phase ammonium aluminate carbonate. The precursor prepared with aluminum chloride as the aluminum source primarily consists of ammonium aluminate carbonate, with minor amounts of boehmite. However, the precursor prepared from aluminum sulfate has a smaller particle size and severe aggregation. This is because, during the reaction process, some aluminum sulfate reacts with ammonium bicarbonate to form aluminum ammonium sulfate, as shown in the chemical reaction in Equation (9). The formation of aluminum ammonium sulfate, on the one hand, reduces the concentration of reactants, preventing the growth of crystal particles. On the other hand, as a coagulant, it promotes the aggregation of small particle crystals [23]. The precursors prepared from aluminum chloride and aluminum nitrate have similar particle sizes, and their surfaces

appear rough, indicating that chloride ions and nitrate ions have no significant impact on the precursor morphology.

$$2Al_2(SO_4)_3 + 3NH_4HCO_3 = 3NH_4Al(SO_4)_2 + Al(OH)_3 \downarrow + 3CO_2 \uparrow \quad (9)$$



(**a**) (**b**) (**c**)

Figure 7. XRD patterns of alumina precursors prepared from different aluminum sources. (**a**) Aluminum sulfate; (**b**) aluminum chloride; (**c**) aluminum nitrate.

The precursor prepared with aluminum sulfate is sodium basic aluminum ammonium carbonate, with an average crystal grain size of 18.11 nm; the precursor prepared with aluminum chloride is sodium basic aluminum ammonium carbonate, with an average crystal grain size of 20.03 nm; the precursor prepared with aluminum nitrate is sodium basic aluminum ammonium carbonate, with an average crystal grain size of 15.26 nm. The average grain size of alumina precursors prepared from different aluminum sources is shown in Table 3.

Table 3. Average crystal grain size of aluminum oxide precursors prepared with different aluminum sources. (a) Aluminum sulfate; (b) aluminum chloride; (c) aluminum nitrate.

Aluminum Sources	Lattice Parameters (Å)	Average Crystalline Size, D (nm)
(a)	$NH_4Al(OH)_2CO_3$ (a = 6.6, b = 11.9, c = 5.7)	18.11
(b)	γ-AlOOH (a = 3.7, b = 12.2, c = 2.8) $NH_4Al(OH)_2CO_3$(a = 6.6, b = 11.9, c = 5.7)	20.03
(c)	$NH_4Al(OH)_2CO_3$ (a = 6.6, b = 11.9, c = 5.7)	15.26

Since the aluminum oxide precursors prepared from the three different aluminum sources are mainly aluminum aluminate carbonate, their TG-DTG curves are similar. From Figure 8, it can be observed that the mass change before 259 °C, 279 °C, and 276 °C is attributed to the removal of adsorbed water and thermal decomposition. After 259 °C, 279 °C, and 276 °C, the mass change is caused by the removal of crystalline water from the aluminum oxide precursor. There is a mass loss of 68%, 63%, and 65%, respectively, on the TG curves, which corresponds to the theoretical mass loss of 63.3% when aluminum aluminate carbonate decomposes into aluminum oxide.

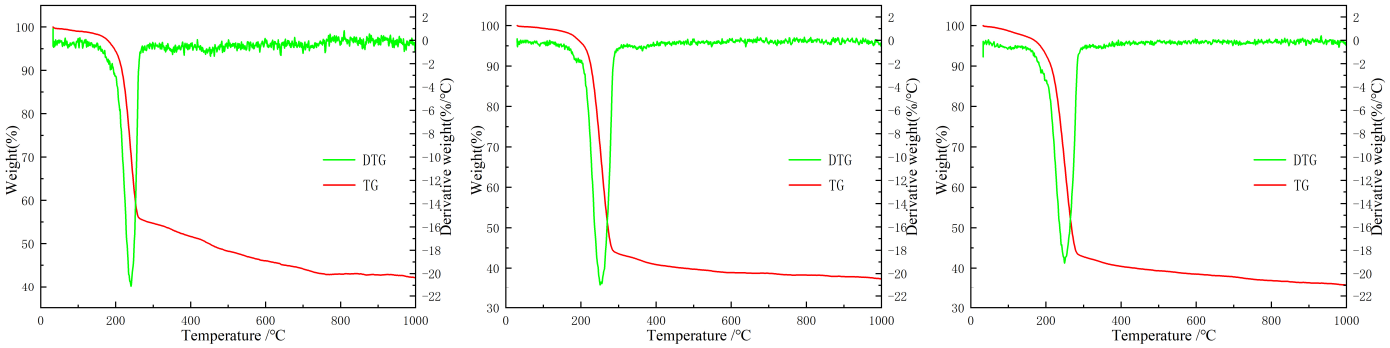


Figure 8. The TG-DTG curves of alumina precursors prepared from different aluminum sources. (**a**) Aluminum sulfate; (**b**) aluminum chloride; (**c**) aluminum nitrate.

3.4. Influence of the Aluminum Source Type on the Morphology of the Aluminum Oxides

To further investigate the impact of the precursors on the microstructure of the aluminum oxide, SEM analysis was conducted on the products obtained after calcination of the precursors prepared from different aluminum sources. The test results are shown in Figure 9.

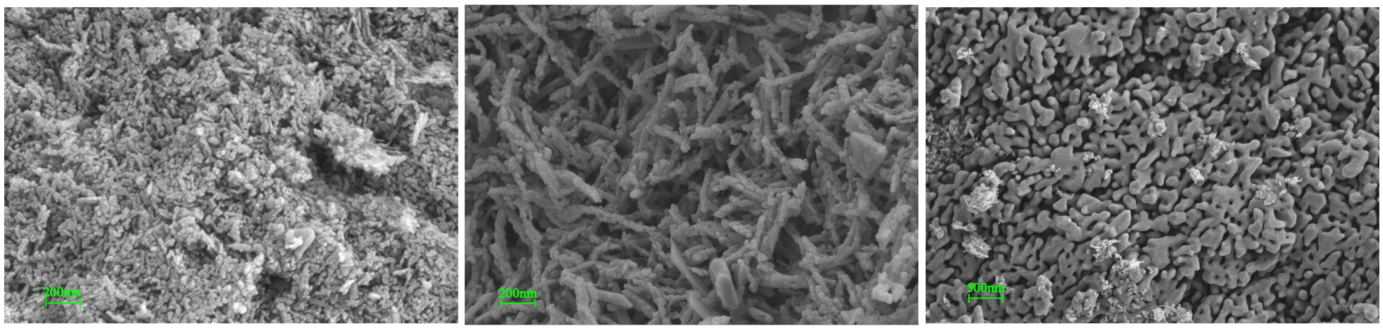


Figure 9. SEM images of alumina prepared from different aluminum sources. (**a**) aluminum sulfate; (**b**) aluminum chloride; (**c**) aluminum nitrate.

Figure 9 clearly shows that there are significant differences in the crystal morphology of the aluminum oxides prepared from the different aluminum sources. The aluminum oxide product prepared from aluminum sulfate has fine particles, often appearing as aggregates, with individual crystallite sizes in the range of 60 to 80 nm. This is due to the small particle size of its precursor, which has higher reactivity. During calcination, the crystals tend to aggregate to reduce the surface energy, and the poor dispersibility of the precursor is a major contributing factor to this phenomenon. On the other hand, the aluminum oxide prepared from aluminum nitrate exhibited a fused appearance. This is because, during the preparation of the precursor, some ammonium nitrate is formed. The solubility of ammonium nitrate is much greater than that of ammonium chloride and aluminum ammonium sulfate. Ammonium nitrate readily adsorbs onto the precursor surface through hydrogen bonding or physical adsorption. Even after multiple centrifuge washes, some residue remains, leading to the role of a fluxing agent during calcination and causing the surface of the aluminum oxide to appear in a fused state [24].

The N_2 adsorption–desorption results are shown in Figure 10. The curves in the N_2 adsorption–desorption isotherm plot exhibit a type IV adsorption branch with an H3 hysteresis loop. According to the BJH calculation, as shown in the pore size distribution curve, these shapes indicate the presence of a significant amount of mesopores. The specific surface area of alumina prepared with aluminum sulfate (68.54 m^2/g) is higher than that

prepared with aluminum chloride (27.07 m^2/g) and aluminum nitrate (6.34 m^2/g). This indicates that alumina prepared with aluminum sulfate possesses abundant active sites and superior adsorption capacity.

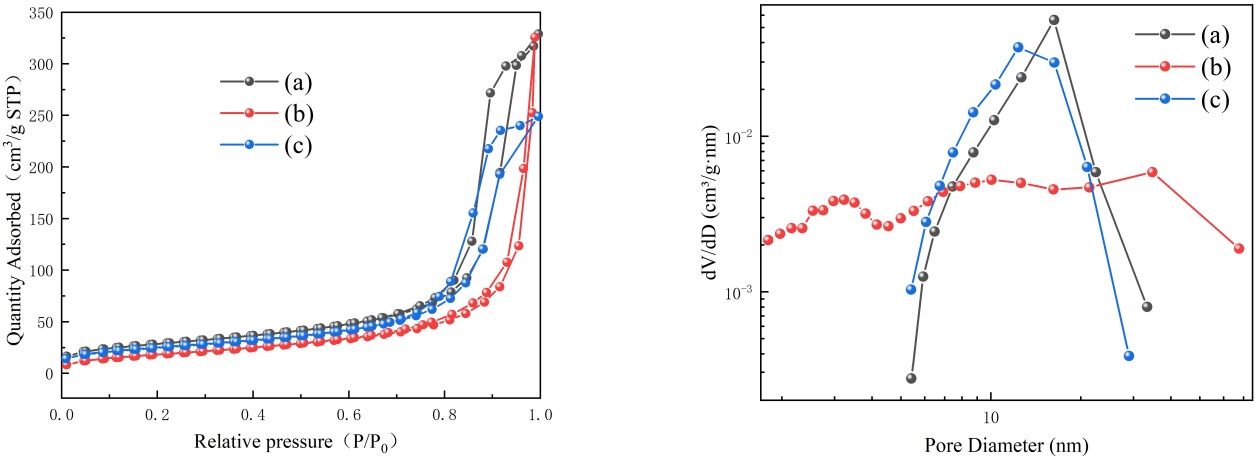
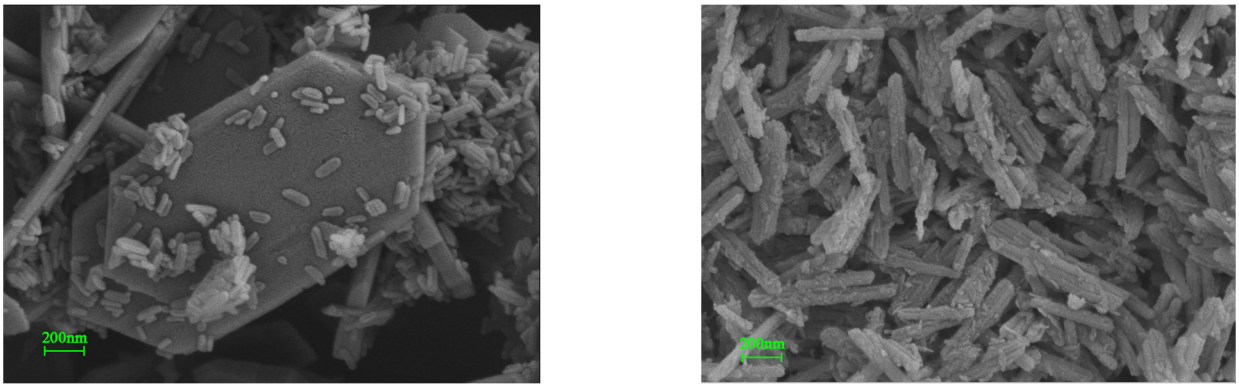


Figure 10. Nitrogen adsorption–desorption isotherms and BJH pore size distribution plots of alumina prepared with different aluminum sources. (a) Aluminum sulfate; (b) aluminum chloride; (c) aluminum nitrate.

3.5. Influence of Reactant Addition Order on the Precursor Morphology of Aluminum Oxide

To further investigate the impact of the order of addition of the reactants on the precursor morphology of aluminum oxide, this study utilized hexahydrate aluminum chloride and ammonium bicarbonate as raw materials. This research focused on exploring the influence of the order of reactant addition on the precursor and microstructure of aluminum oxide. The test results are presented in Figures 11 and 12.



(**a**) (**b**)

Figure 11. SEM images of alumina precursors prepared by different agent addition sequences. (**a**) Aluminum chloride added dropwise to ammonium bicarbonate; (**b**) ammonium bicarbonate added dropwise to aluminum chloride.

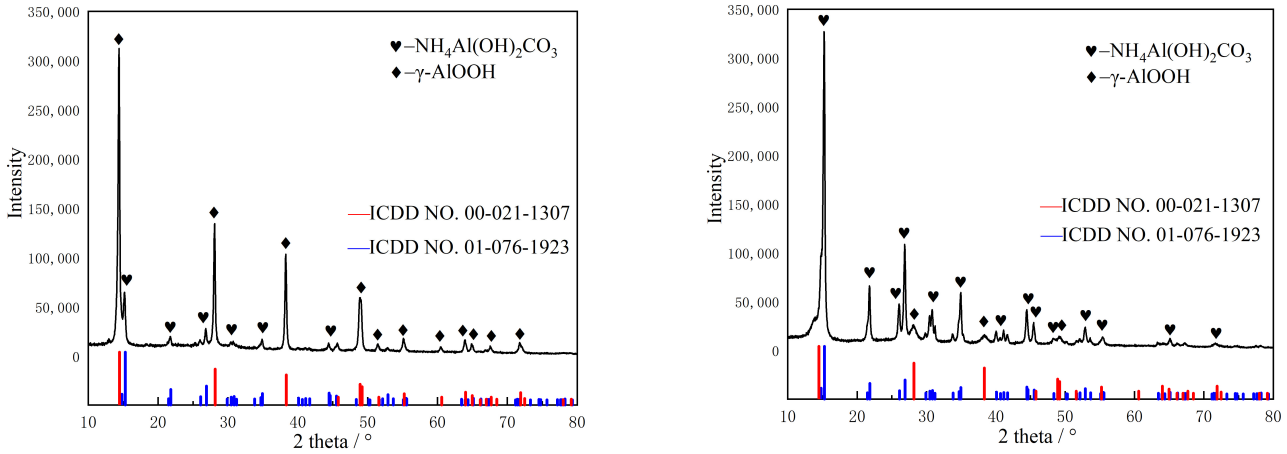


Figure 12. XRD patterns of alumina precursors prepared by different agent addition sequences. (**a**) Aluminum chloride added dropwise to ammonium bicarbonate; (**b**) ammonium bicarbonate added dropwise to aluminum chloride.

When aluminum chloride was added dropwise to ammonium bicarbonate, the precursor primarily consisted of boehmite, with an average crystal grain size of 26.69 nm. When ammonium bicarbonate was added dropwise to aluminum chloride, the precursor primarily consisted of sodium basic aluminum ammonium carbonate, with an average crystal grain size of 20.03 nm. The grain size of alumina precursors prepared in different addition orders is shown in Table 4.

Table 4. Crystal grain size of aluminum oxide precursors prepared with different addition sequences. (a) Aluminum chloride added dropwise to ammonium bicarbonate; (b) Ammonium bicarbonate added dropwise to aluminum chloride.

Addition Order	Lattice Parameters (Å)	Average Crystalline Size, D (nm)
(a)	γ-AlOOH (a = 3.7, b = 12.2, c = 2.8)	26.69
(b)	$NH_4Al(OH)_2CO_3$(a = 6.6, b = 11.9, c = 5.7)	20.03

From Figure 13a, it can be observed that there are two peaks at 100 °C and 300 °C in the DTG curve, which are likely caused by the removal of excess water molecules with different binding energies from the surface and interlayers of boehmite. The sharp decrease in the TG curve at 431 °C is attributed to the transformation of boehmite into γ-alumina. As shown in Figure 13b, the DTG curve indicates that the mass change before 279 °C is due to the removal of adsorbed water and thermal decomposition, while the mass change after 279 °C is caused by the removal of crystalline water from the aluminum oxide precursor. According to the TG curves of aluminum aluminate carbonate and boehmite, it can be inferred that aluminum aluminate carbonate is more readily converted into α-alumina compared to boehmite.

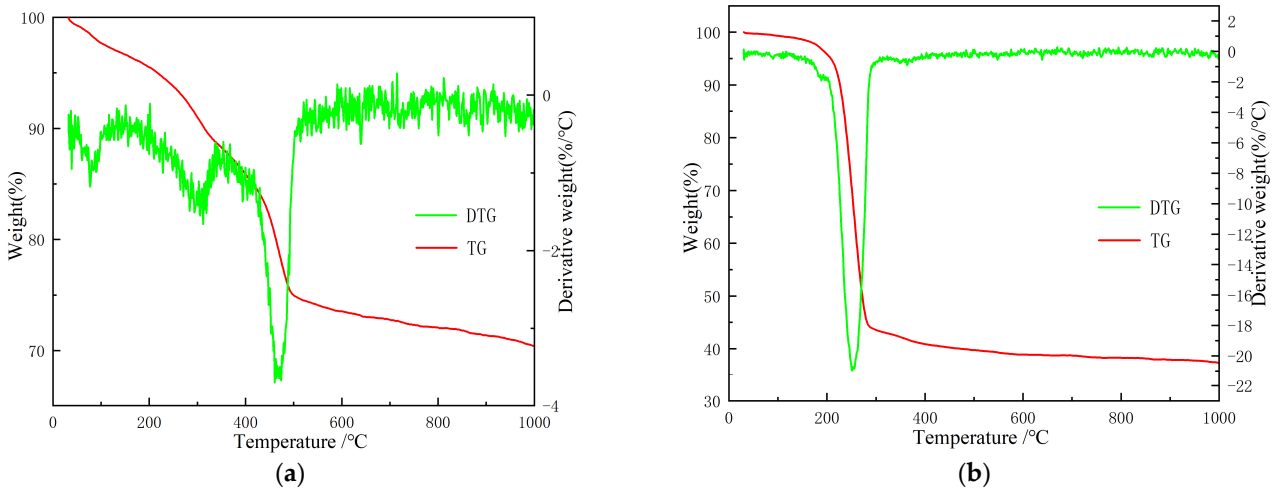


Figure 13. The TG-DTG curves of alumina precursors prepared by different agent addition sequences. (**a**) Aluminum chloride added dropwise to ammonium bicarbonate; (**b**) ammonium bicarbonate added dropwise to aluminum chloride.

From Table 1 and Figures 14 and 15, it can be observed that the precursor prepared by adding an aluminum chloride solution dropwise into an ammonium bicarbonate solution is an irregular rod-shaped sodium basic aluminum ammonium carbonate. On the other hand, the precursor primarily consists of hexagonal boehmite, with a small amount of short rod-shaped sodium basic aluminum ammonium carbonate when ammonium bicarbonate solution is added dropwise into the aluminum chloride solution. This phenomenon may be related to the initial concentration of ions in the solution. When aluminum chloride was added dropwise to the ammonium bicarbonate solution, amorphous aluminum hydroxide was initially formed. Due to the abundance of hydroxyl groups on the surface of amorphous aluminum hydroxide, a high-energy state is created on the surface. At this point in the reaction solution, the concentrations of carbonate ions and ammonium ions are much greater than that of aluminum ions. Amorphous aluminum hydroxide first forms a stable octahedral aluminum–oxygen structure with unsaturated oxygen atoms from carbonate ions in the form of shared oxygen atoms. Subsequently, carbonate ions and ammonium ions form ionic bonds to make the overall structure electrically neutral, reducing their own energy. This process results in the formation of well-defined crystalline sodium basic aluminum ammonium carbonate crystals [23]. From the crystal structure perspective, the apex oxygen atoms of the aluminum–oxygen octahedra are exposed in the direction of the a-axis, forming chains connected in a parallel manner along the a-axis in a vertex-to-vertex arrangement. In contrast, the edges of the aluminum–oxygen octahedra are exposed in the b-axis and c-axis directions, and their growth rate is lower, leading to the overall rod-shaped growth of the crystal, as shown in Figure 14.

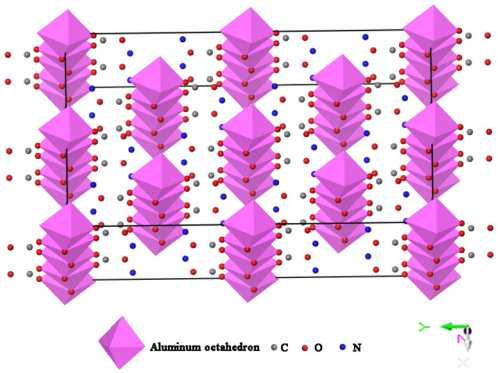


Figure 14. Schematic diagram of the crystal structure of ammonium aluminum carbonate hydroxide.

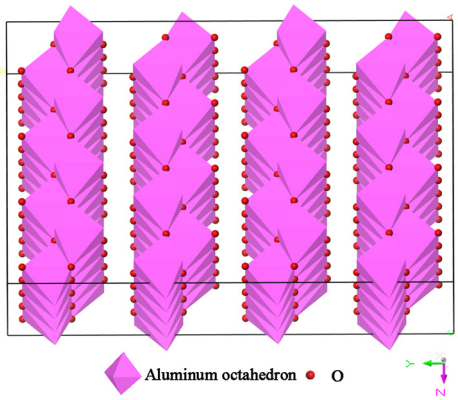
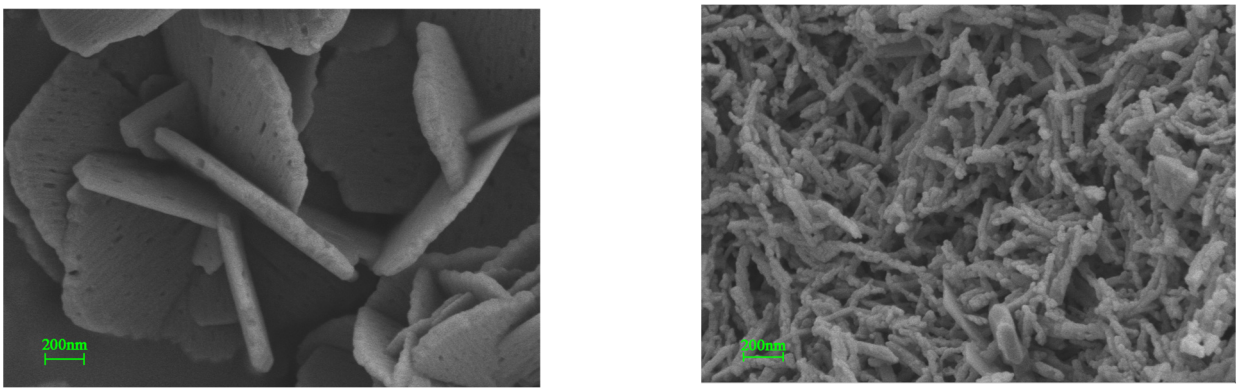


Figure 15. Schematic diagram of boehmite crystal structure.

When ammonium bicarbonate was added dropwise to the aluminum chloride solution, amorphous aluminum hydroxide was generated. Although amorphous aluminum hydroxide creates a high-energy state on the surface due to the abundance of hydroxyl groups, the limited quantity of carbonate ions in the solution results in only a small amount of amorphous aluminum hydroxide forming a stable octahedral aluminum–oxygen structure with unsaturated oxygen atoms from carbonate ions. Most of the reactions involve dehydration condensation, leading to the formation of an aluminum–oxygen octahedral stable structure. In this structure, the vertices of the octahedra consist of oxygen atoms arranged in a face-centered cubic manner to form layers. The remaining hydroxyl groups on the octahedra surfaces connect the layers through hydrogen bonds, resulting in an ordered layered structure. From the crystal structure perspective, boehmite can develop into plate-like crystals along the a-axis and into the c-axis or rod-like crystals along the b-axis, as shown in Figure 15.

3.6. Influence of the Reactant Addition Order on the Morphology of the Aluminum Oxides

The experimental results from Sections 3.2 and 3.4 reveal that there is a certain inheritance relationship between the precursor morphology and the morphology of the aluminum oxide. Figure 16 shows the microscopic morphology of aluminum oxide prepared with different reactant addition sequences. When an aluminum chloride solution was added dropwise to the ammonium bicarbonate solution, the aluminum oxide morphology after high-temperature calcination appeared as hexagonal plates with long sides and short angles, with a thickness of approximately 100 nm and a radial size of approximately 1200 nm. During the calcination process, boehmite undergoes dehydration, changing from a dense crystal face to a porous crystal face, but the overall morphology remains largely unchanged. A small amount of sodium basic aluminum ammonium carbonate in the precursor decomposes under heat and is absorbed by the growth of hexagonal plate-shaped aluminum oxide crystals. In contrast, when ammonium bicarbonate solution was added dropwise to the aluminum chloride solution, the morphology of the aluminum oxide was primarily rod shaped. During the calcination process, sodium basic aluminum ammonium carbonate decomposes under heat, transforming from irregular rod-shaped structures with a length of approximately 800 nm and a diameter of approximately 60 nm to short rod-shaped aluminum oxide structures with a length of approximately 200 nm.



(**a**) (**b**)

Figure 16. SEM images of alumina prepared by different agent addition sequences. (**a**) Aluminum chloride added dropwise to ammonium bicarbonate; (**b**) ammonium bicarbonate added dropwise to aluminum chloride.

The N_2 adsorption–desorption results are shown in Figure 17. The curves in the N_2 adsorption–desorption isotherm plot exhibit a type IV adsorption branch with an H3 hysteresis loop. According to the BJH calculation, as shown in the pore size distribution curve, these shapes indicate the presence of a significant amount of mesopores. The specific surface area of alumina prepared by adding aluminum chloride dropwise to ammonium bicarbonate (68.54 m^2/g) is higher than that prepared by adding ammonium bicarbonate dropwise to aluminum chloride (48.01 m^2/g). This indicates that alumina prepared by adding aluminum chloride dropwise to ammonium bicarbonate possesses abundant active sites and superior adsorption capacity.

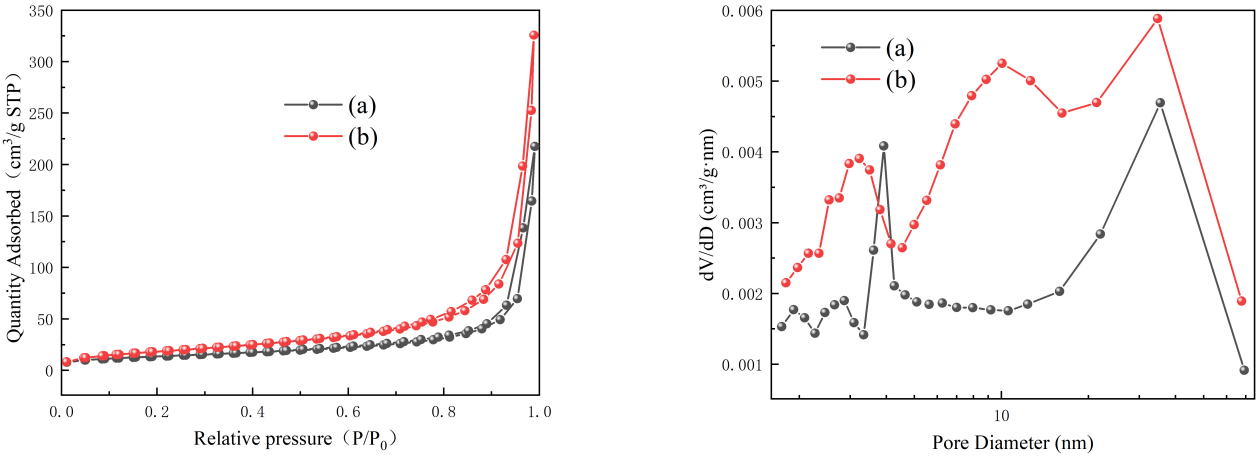


Figure 17. N_2 adsorption–desorption isotherms and BJH pore size distribution plots of alumina prepared with different addition sequences. (a) Aluminum chloride added dropwise to ammonium bicarbonate; (b) ammonium bicarbonate added dropwise to aluminum chloride.

4. Conclusions

This paper investigated the impact of reactant type and addition sequence on the microscopic morphology of aluminum oxide. Three aluminum sources, namely, octadecahydrated aluminum sulfate, hexahydrated aluminum chloride, and nonahydrated aluminum nitrate, were employed along with precipitants such as ammonium bicarbonate, sodium bicarbonate, and potassium bicarbonate. Precursors were synthesized using a hydrothermal method, and aluminum oxide powders were prepared through calcination. The key findings are summarized as follows:

1. Using sodium bicarbonate, ammonium bicarbonate, and potassium bicarbonate as precipitants and hexahydrated aluminum chloride as the aluminum source, spherical aluminum oxide particles with an average diameter of 80 nm were prepared. These particles exhibited mutual adhesion. Additionally, irregular short rod-shaped aluminum oxide with a length of approximately 200 nm and hexagonal plate-shaped aluminum oxide with long sides and short angles were obtained.
2. Using octadecahydrate aluminum sulfate, hexahydrate aluminum chloride, and nonahydrate aluminum nitrate as aluminum sources and ammonium bicarbonate as a precipitant, single-crystal particles of aluminum oxide were prepared. These particles had diameters ranging from 60 to 80 nm but tended to aggregate. Additionally, irregular short rod-shaped aluminum oxide with a length of approximately 200 nm and molten-adhered aluminum oxide were obtained.
3. The order of reactant addition significantly influences the crystal precursor products. Using hexahydrated aluminum chloride and ammonium bicarbonate as raw materials, when aluminum chloride was dripped into the ammonium bicarbonate solution, the resulting precursor was mainly sodium aluminum hydroxide carbonate, with some boehmite present. On the other hand, when ammonium bicarbonate was dripped into the aluminum chloride solution, the primary precursor formed was boehmite, which contained a small amount of sodium aluminum hydroxide carbonate. After calcination, the boehmite underwent dehydration, transitioning from a dense plate-like structure to a porous plate-like aluminum oxide, maintaining its overall morphology. Conversely, sodium aluminum hydroxide carbonate transformed from irregular rod-shaped structures with a length of 800 nm and a diameter of 60 nm into short rod-shaped aluminum oxide structures with a length of approximately 200 nm, indicating a reduction in size.

Author Contributions: Conceptualization, W.W. and Y.B.; methodology, W.W., Y.B. and P.Y.; formal analysis, W.W. and Y.B.; resources, Y.G. and H.X.; data curation, W.W., M.X. and Y.B.; writing—original draft preparation, W.W.; writing—review and editing, Y.B.; supervision, P.Y. and Y.G. All authors have read and agreed to the published version of the manuscript.

Funding: This research was funded by the National Natural Science Foundation of China (Project No. 51674137) and the Natural Science Foundation of Shandong Province (Project No. ZR2022ME013) are sincerely appreciated. And the APC was funded by the Natural Science Foundation of Shandong Province (Project No. ZR2022ME013).

Institutional Review Board Statement: Not applicable.

Informed Consent Statement: Not applicable.

Data Availability Statement: The raw data supporting the conclusions of this article will be made available by the authors on request.

Conflicts of Interest: The research was conducted in the absence of any commercial or financial relationships that could be construed as potential conflicts of interest.

References

1. Wang, P.F.; Yang, H.L.; Li, J.Y.; Zhang, X.H.; Wang, L.; Xiao, J.C.; Zhao, B. Synergistically enhanced performance and reliability of abrupt metal-oxide heterojunction transistor. *Adv. Electron. Mater.* **2023**, *9*, 2200807. [CrossRef]
2. Komrakova, S.; An, P.; Kovalyuk, V.; Golikov, A.; Gladush, Y.; Mkrtchyan, A.; Chermoshentsev, D.; Krasnikov, D.; Nasibulin, A.; Goltsman, G. Hybrid Silicon Nitride Photonic Integrated Circuits Covered by Single-Walled Carbon Nanotube Films. *Nanomaterials* **2023**, *13*, 2307. [CrossRef]
3. Nabiullina, R.D.; Nikitin, I.Y.; Soloveva, E.O.; Gladskikh, I.A.; Starovoytov, A.A. Optical properties of nanoporous aluminum oxide activated by molecular clusters of pseudoisocyanine dye. *Nanophotonics* **2022**, *12131*, 170–174.
4. Rheima, A.M.; Sabri, A.Z.; Kadhim, M.M.; Mohammed, S.H.; Alhameedi, D.Y.; Rasen, F.A.; Ramadan, M.F.; Abed, Z.T.; Jaber, A.S.; Hachim, S.K.; et al. Aluminum oxide nano porous: Synthesis, properties, and applications. *Case Stud. Chem. Environ. Eng.* **2023**, *8*, 100428. [CrossRef]
5. Zhang, W. Preparation and Characterizations of Monodisperse α-Al_2O_3 Nanospheres. Master's Thesis, Lanzhou University, Lanzhou, China, 2016.

6. Gurel, S.B.; Altun, A. Reactive alumina production for the refractory industry. *Powder Technol.* **2009**, *196*, 115–121. [CrossRef]
7. Fruhstorfer, J.; Schöttler, L.; Dudczig, S.; Schmidt, G.; Gehre, P.; Aneziris, C.G. Erosion and corrosion of alumina refractory by ingot casting steels. *J. Eur. Ceram. Soc.* **2016**, *36*, 1299–1306. [CrossRef]
8. Qin, L.P.; Gu, Y.Y.; Ye, H.Q. The Selection of Molten Salts in Synthesizing Flaky Alumina by Using Molten-salt. *China Chem.* **2005**, *6*, 35–38.
9. Zhou, X.L.; Xu, J.Y.; Sun, J.H.; Cao, A.L.; Qing, P.L. Study on the Preparation of Flake α-Al_2O_3 Based on Molten Salt and Liquid Meta. *China Ceram.* **2023**, *59*, 29–35.
10. Xu, N.C.; Shi, D.D. Research on preparation of mesoporous alumina nanomaterials and their fluoride removal properties. *Appl. Chem. Ind.* **2023**, *52*, 464–470.
11. Xu, H.; Zhang, C.; Cai, J.; Wang, J.; Liu, K.; Cheng, X. Synthesis and characterization of activated alumina with high thermal stability by a low-heat solid-phase precursor method. *Microporous Mesoporous Mater.* **2022**, *337*, 111921. [CrossRef]
12. Shen, Y.Q.; Li, D.Y.; Xu, Y.; Ge, H.L.; Yang, H. Influence mechanism of halide additives on phase conversion, morphology, and purity of alumina powders prepared by solid-phase calcination method. *Ceram. Int.* **2022**, *48*, 8403–8408.
13. Vasile, B.S.; Birca, A.C.; Surdu, V.A.; Neacsu, I.A.; Nicoară, A.I. Ceramic composite materials obtained by electron-beam physical vapor deposition used as thermal barriers in the aerospace industry. *Nanomaterials* **2020**, *10*, 370. [CrossRef]
14. Konstantiniuk, F.; Tkadletz, M.; Kainz, C.; Czettl, C.; Schalk, N. Mechanical properties of single and polycrystalline α-Al_2O_3 coatings grown by chemical vapor deposition. *Surf. Coat. Technol.* **2021**, *410*, 126959. [CrossRef]
15. Lee, J.S.; Kim, H.S.; Park, N.K.; Lee, T.J.; Kang, M. Low temperature synthesis of α-alumina from aluminum hydroxide hydrothermally synthesized using [Al(C_2O_4)x(OH)y] complexes. *Chem. Eng. J.* **2013**, *230*, 351–360. [CrossRef]
16. Xu, K.J.; Yang, X.C.; Tian, G.S. Preparation of nano-size α-Al_2O_3 powders by seeding hydrothermal synthesizing method. *J. Chin. Ceram. Soc.* **2001**, *6*, 576–579.
17. Pallavi, S.B.; Sunipa, B.; Thermal, D. phase evolution and morphology study of combustion synthesized alumina powder—Influence of precursor Ph. *Mater. Chem. Phys.* **2021**, *259*, 124030.
18. Chang, Y.; Zhang, A.F.; Guo, X.W.; Shang, S.J.; Zhang, J.X. Morphological control of mordenite and its performance in alkylation reaction. *Mod. Chem. Ind.* **2023**, *43*, 219–224.
19. Zhang, B. Optimized Preparation and Pervaporation Performance of T Zeolite Membrane. Master's Thesis, Dalian University of Technology, Dalian, China, 2020.
20. Liu, D.M.; Li, S.K.; Tang, J.J.; Zhou, N.; Zhong, M.E. Impact Factors on Morphology and Particle Size of Lithium Vanadium Phosphate during Solvothermal Synthesis. *Guangzhou Chem. Ind.* **2019**, *47*, 55–58.
21. Yu, Q.Q. Preparation of Alumina Adsorbent with High-Surface-Area and the Removal of Cr(VI). Master's Thesis, Beijing University of Chemical Technology, Beijing, China, 2017.
22. Dai, X.; Bai, J.; Huang, Q.; Liu, Z.; Bai, X.; Cao, R.; Wen, X.; Li, W.; Du, S. Viscosity temperature properties from molecular dynamics simulation, The role of calcium oxide, sodium oxide and ferrous oxide. *Fuel* **2019**, *237*, 163–169. [CrossRef]
23. Wang, Z.; Chen, X.H.; Li, D.H.; Hu, W.H. Study on the preparation and growth mechanism of ammonium aluminum carbonate. *J. Chin. Soc. Rare Earths* **2012**, *4*, 397–400.
24. Tripathy, A.K.; Ray, H.S.; Pattnayak, P.K. Kinetics of roasting of chromium oxide with sodium nitrate flux. *Metall. Mater. Trans. B* **1995**, *26*, 449–454. [CrossRef]

Disclaimer/Publisher's Note: The statements, opinions and data contained in all publications are solely those of the individual author(s) and contributor(s) and not of MDPI and/or the editor(s). MDPI and/or the editor(s) disclaim responsibility for any injury to people or property resulting from any ideas, methods, instructions or products referred to in the content.